Multifractality in the Copolymerization of Bis-GMA/TEGDMA by Pulsed Photoacoustics

M. Navarrete,[1] J. Pineda,[2] R. Vera-Graziano[3]

[1]*Instituto de Ingeniería, Universidad Nacional Autónoma de México, Av. Universidad 3000, C. P. 04510, D. F., México*
[2]*Facultad de Ciencias, Universidad Nacional Autónoma de México, Av. Universidad 3000, C. P. 04510, D. F., México*
[3]*Instituto de Investigaciones Materiales, Universidad Nacional Autónoma de México, Av. Universidad 3000, C. P. 04510, D. F., México*

Received 17 October 2007; accepted 4 July 2008
DOI 10.1002/app.28992
Published online 22 October 2008 in Wiley InterScience (www.interscience.wiley.com).

ABSTRACT: Fractal development during polymerization of a dimethacrylate system (Bis-GMA/TEGDMA) has been studied through the analysis of time series obtained sequentially by pulsed photoacoustics. The photoacoustic signals as obtained *in situ* during photopolymerization of Bis-GMA/TEDGMA were analyzed by rescaled range analysis, dispersion analysis, and detrended fluctuation analysis methods. The analysis reveals the presence of more than one scaling parameter and, therefore, belongs to a complex process known as multifractal. The evolution of fractality during photopolymerization was compared under equivalent conditions with the chemical conversion (of dimethacrylate double bonds) as a function of time, as monitor by infrared spectroscopy. This kinetic study was also used to correlate the fractal nature of the dimethacrylate reaction system with the condensed-state transitions emerging during the photochemical reaction. © 2008 Wiley Periodicals, Inc. J Appl Polym Sci 111: 1199–1208, 2009

Key words: curing polymers; photopolymerization; microgels; networks, fractal analysis

INTRODUCTION

In general, dental composite resins are mostly based on mixtures of dimethacrylate monomers and promoters that rapidly polymerize under visible light (photopolymerization). The most common used monomer is the 2,2-bis[4-(2-hydroxy-methacryloxy-propoxy)phenyl]propane (Bis-GMA). Both, the molecular structure of Bis-GMA (aromatic rings) and its hydrogen bonding capability (with hydroxyl groups) promote sufficient strength after the material is polymerized. However, Bis-GMA handling during dental restorations is troublesome because of its high viscosity.[1] To increase fluidity and to enhance the formation of a three-dimensional molecular network (by crosslinking) triethylene-glycol-dimethacrylate (TEGDMA) is usually mixed with Bis-GMA.[2,3] The photopolymerization reaction involves conversion of the double bonds of the methacrylate groups of both, Bis-GMA and TEGDMA, by a free radical mechanism. The degree of chemical conversion of these double bonds commonly ranges from 50 to 85%, some of them are used for crosslinking, and others remain as part of side chains, affecting the mechanical response of the dental resin and reducing its hydrolytic resistance and color stability.

The kinetics of polymerization and the morphology of the resulting copolymers have been analyzed by using different techniques reported elsewhere, such as: differential scanning calorimetry; thermomechanical analysis; ultrasonic wave propagation[4–6]; FTIR, RTIR, NMR, and Raman spectroscopies[7–10]; plasma light[11]; and impulsive stimulated thermal scattering,[12] where measurements of elastic properties on real time conditions, during Bis-GMA polymer processing, are possible with laser acoustic techniques.

After Carothers,[13] many theories have been developed to describe the molecular processes during gel formation in several polymerization reactions. The classical gelation theory was developed by Flory and Stockmayer,[14,15] who established the background for further developments. In fact, there are several models which can explain network formation, such as kinetic models,[16–20] statistical models,[21,22] hybrid models, and computer simulation models.[23] The most prominent of the *n*-dimensional network theories is the percolation model that it is associated with a lattice and uses a Monte Carlo Technique.[24–26] Some statistical theories of gelation assume

Correspondence to: M. Navarrete (mnm@pumas.iingen.unam.mx).

Contract grant sponsor: DGAPA-UNAM; contract grant number: IN103706.

thermodynamic equilibrium; however, the development of chain properties depends strongly on the reaction path. This means that the growth process phenomena are far-from-equilibrium. For this reason, the methods of fractal geometry are increasingly used.[27–30]

The methods of fractal geometry allow the classification of nonequilibrium growth processes according to their scaling properties. This classification and computer simulations give insight into a great variety of complex structures.

As it is known, by using methods of fractal analysis as well as irreversible and aggregation models, it has been determined that crosslinking may occur in homogeneous as well as in heterogeneous media.[31–33] From these studies, it has been suggested that network formation proceeds in two steps: first step is characterized by polymerization and formation of microgels and second step by the connection among microgels, resulting in a tridimensional network.[8,34–36] During the first step, the system turns from a fluid monomer to a homogeneous viscoelastic polymer, where microgels form nearly up to the point of gelation. This step is also characterized by a constant value of the fractal dimension. During the second step, the system turns from a viscoelastic to an elastic polymer, where macrogels are formed by a heterogeneous crosslinking reaction. This step is also characterized by a monotonous growth of the fractal dimension.[28–33]

The fundamentals of the pulsed photoacoustics technique to study solid or/liquid samples are well established[37]; the photoacoustic signal (PA signal) critically depends on the thermoelastic and physical properties of the material and have been widely used for materials characterization using pulsed lasers and piezoelectric sensors.[38–41]

Here, a pulsed laser was used as a standard source of ultrasound to monitor the photopolymerization process (PP process) as a function of reaction time. Data series obtained by photoacoustic and generated during the PP process can exhibit fluctuations on a wide range of time scales and/or broad distributions of the values. In both equilibrium and nonequilibrium situations, the natural fluctuations are often found to follow a scaling relation over several orders of magnitude. Such dynamics are usually denoted as fractal or multifractal depending on the question if they are characterized by one scaling exponent or by a multitude of scaling exponents. Phase transitions are often associated with changes in their fractal dynamics, allowing for a detection of such transitions (or corresponding states) by fractal analysis. To observe fractal and multifractal scaling behavior in time series, several tools have been developed. For our case, the fractal properties were obtained by applying the PA signals to the following methods: rescaled range analysis (R/S), dispersional analysis (DA), and detrended fluctuation analysis (DFA). Conversion from monomer to polymer was also monitored on real time conditions by infrared techniques.

Fractal development during the PP process are discussed first, then the obtained results are compared among them and finally against the conversion of acrylic group double bonds on real time conditions.

METHODS USED TO STUDY FRACTAL NATURE

Glossary

Time series

One-dimensional array of numbers (x_i), $i = 1,\ldots,N$, representing values of an observable x usually measured equidistant (or nearly equidistant) in time.

Fractal time series

A fractal object is defined as one that shows self-similarity or self-affinity independent of scaling. For a function $f(t)$ to be self-similar both $f(t)$ and t must have the same units, temporal: e.g., electrocardiographic R–R intervals versus time. As a general time series $f(t)$ has units of amplitude in volts, distance, etc., versus units of time it cannot be self-similar but is termed self-affine. Self-affinity implies, therefore, that the roughness or variability of the signal is independent of Δt, where the time interval Δt, is a measure of the temporal resolution. Self-affine signals have power law spectra—a proportional increment in frequency predicts a proportional decrement in power, independent of the frequency.[42]

Fractal dimension

Fractal dimensions have multiple definitions, but all have a thing in common: the fractal dimension is usually a noninteger, fractional number; hence, this dimension is referred to as fractal. The existing fractal dimensions include Hausdorff dimension, box dimension, information dimension, correlation dimension, and so on.

Geometric dimension of an object which includes fractal objects

For a smooth (i.e., nonfractal) line, an approximate length $L(r)$ is given by the minimum number N of segments of length r needed to cover the line: $L(r) = Nr$. As r goes to zero, $L(r)$ approaches a finite limit, the length L of the curve. Similarly, it is possible to

define the area A or the volume V of nonfractal objects as the limit of an integer power law of r:

$$A = \lim_{r\to 0} Nr^2, \quad V = \lim_{r\to 0} Nr^3$$

where the integer exponent is the Euclidean dimension E of the object.

However, this definition cannot be used for fractal objects: as r tends to 0, however, a real number D exists so that the limit of Nr^D stays finite. The exponent is called the Hausdorff Dimension D_H or D:

$$D_H \equiv \lim_{r\to 0} \frac{\log N}{\log(1/r)}$$

Another popular definition of dimension proposed for fractal objects is the Correlation Dimension, D_c

$$D_c \equiv \lim_{r\to 0} \frac{\log C(r)}{\log(r)}$$

where $C(r)$ is the number of points which have a smaller (Euclidean) distance than a given distance r.

D_c may also be used to determine whether a timeseries derives from a random process or from a deterministic chaotic system. M-dimensional data vectors are constructed from m measurements spaced equidistant in time, and D_c is evaluated for this m-dimensional set of points. If the timeseries is a random process, D_c increases with m; if the timeseries is a deterministic signal, D_c does not increase further when the embedding dimension m exceeds D_c. Thus, a plot of the correlation dimension as a function of the embedding dimension may easily show whether a signal is random noise of deterministic chaos. Note that $D_c \leq D_H$. Another way to calculate the fractal dimension is through the estimation of the Hurst's exponent, H.[43,44]

As suggested elsewhere,[44] at least two different methods are necessary to obtain a faithful representation of fractal nature of the time series. Here, the Hurst's R/S, DA, and a box-counting method DFA were adopted to process the scattered PA signals to study the fractal nature during PP process. The calculations described later were programmed in C language.

Rescaled range analysis

Rescaled range analysis (R/S) analysis was originally developed by Hurst.[45] This procedure provides an approach for the analysis and characterization of timeseries noisy records which has no underlying periodicity but retains the long-term correlation. It is a method for stationary fractal time series analysis.[46–49]

The R/S statistics is the range of partial sums of deviations of a time series from its mean, rescaled by its standard deviation. For a time series $\{x(1), x(2),\ldots, x(t)\}$ of a natural phenomenon recorded at discrete periods over a time span τ, the classical rescaled range is given in terms of the mean, $\overline{x}$ (τ), and the standard deviation, $S(\tau)$:

$$(R/S) = \frac{1}{S(\tau)} \left\{ \operatorname*{Max}_{1<k<\tau} \sum_{j=1}^{k} (x_j - \overline{x}_\tau) - \operatorname*{Min}_{1<k<\tau} \sum_{j=1}^{k} (x_j - \overline{x}_\tau) \right\} \quad (1)$$

Hurst found that the rescaled range observations could be well represented by:

$$(R/S)_\tau = a\tau^H$$

where H is the Hurst exponent and a is a proportionality constant. Using a logarithmic transformation, the Hurst exponent can be estimated using the following regression:

$$\log(R/S)_\tau = \log(a) + H\log(\tau) \quad (2)$$

By plotting log $(R/S)_t$ against log (τ) the scaling region can be obtained; the slope of the straight line, H, is the Hurst exponent. The relationship between the H and the box counting fractal dimension is as follows:

$$D = 2 - H \quad (2a)$$

Dispersional analysis for a one-dimensional signal

This is a method that is applied for stationary or nonstationary fractal time series analysis. Dispersional analysis (DA) analysis involves the measurement of the variance or standard deviation of a signal at a succession of different levels of resolution.[42] The different levels are obtained by grouping adjacent data points and replacing each with the group average. A linear relationship between the log of the standard deviation SD, and the log of the size, m, of the observed unit is given by:

$$\mathrm{SD}(m)/\mathrm{SD}(m_0) = (m/m_0)^{1-D} \quad (3)$$

Or in linear form to determine the fractal dimension D from the slope of the log–log regression:

$$\log[\mathrm{SD}(m)/\mathrm{SD}(m_0)] = (1-D)\log(m/m_0) \quad (4)$$

$$D = 1 - \frac{\log[\mathrm{SD}(m)/\mathrm{SD}(m_0)]}{\log(m/m_0)} \quad (4a)$$

where m is the element size, and m_0 is the reference size arbitrarily chosen.

The fractal dimension D is related to the Hurst exponent H by eq. (2a). H provides a direct indication of the degree of smoothness or correlation with the same meaning for signals of any Euclidean dimension, E. In general, $H = E+1 - D$.

For a signal $f(t)$ measured at even intervals of time: f_i, $i = 1, 2, \ldots, N$ at $t = t_1, t_2, \ldots t_N$ and with a constant time interval Δt between samples, in this case the PA signal, the standard deviation of a set of n observations is calculated as:

$$\mathrm{SD}(m) = \frac{1}{n}\sqrt{\left[n\sum f_i^2 - \left(\sum f_i\right)^2\right]}, \qquad (5)$$

As a first approximation the data set of N points is composed of n groups of points and, in this case, each group consists of one datum. Next, adjacent samples are aggregated into groups, each consisting of two adjacent data points, and group size is set as $m = 2$, or a binning period $\tau = 2\Delta t$. The mean for each pair is calculated as well as the SD of the mean of the groups. Then, the group size m is increased to 4, 8, 16, 32, etc., until the number of groups, n, ≤ 4 (it is advisable to begin with four data by group), for each grouping $m \times n = N$.

A good approximation of the fractal dimension is obtained by plotting log SD(m) versus log m. A straight line plot indicates a simple fractal. A measure of the confidence limits on the slope is determined by calculating the standard linear regression. We chose $m_0 = 1$, must be the chosen. The fractal dimension, D, is calculated from the slope of the power law plot: the estimated D is $<D> = (1 -$ slope), as in eq. (4a). Equivalently, the estimated H is $<H> =$ (slope + 1).

Detrended fluctuation analysis

Detrended fluctuation analysis (DFA) was developed to accurately quantify long-range power-law embedded in a nonstationary time series.[50,57] This method provides a single quantitative parameter–the scaling exponent α-, a self-similarity parameter that represents the long-range power law correlation properties of a signal.

The DFA method has been well described elsewhere.[50–53,56] Briefly, given a time series, $x(i)$, where $i = 1,\ldots, N_{\max}$, where $N_{\max}$ is the length of the signal, the integrated signal $y(k)$ is given by:

$$y(k) = \sum_{i=1}^{k}[x(i) - \langle x\rangle], \qquad (6)$$

where $\langle x\rangle$ is the mean. The integrated signal $y(k)$ is divided into boxes of equal length n. In each box $y(k)$ is fitted by using a polynomial function of order l, which represents the trend for that box. The y coordinate of the fitted line in each box is y_n(k).

The integrated signal $y(k)$ is detrended by subtracting the local trend $y_n(k)$ in each box. For a given n size box, the root-mean-square (rms) fluctuation for this integrated and detrended signal is calculated by:

$$F(n) \equiv \sqrt{\left(\frac{1}{N_{\max}}\sum_{k=1}^{N_{\max}}[y(k) - y_n(k)]^2\right)} \qquad (7)$$

The procedure described earlier is repeated for a broad range of scales to provide a relationship between $F(n)$ and the box size n. A power-law relationship between $F(n)$ and the box of size n indicates the presence of scaling: $F(n) \sim n^{\alpha}$. The fluctuations can be characterized by a scaling exponent α, a parameter that represents the long-range power-law correlation properties of the signal.[54]

For uncorrelated data, the integrated value $y(k)$ corresponds to a random walk and therefore, $\alpha = 0.5$. A value of $0.5 < \alpha < 1.0$ indicates the presence of long memory so that a large value is more likely to be followed by a large value and vice versa. In contrast, $0 < \alpha < 0.5$ indicates a different type of power-law correlations such that large and small values of time series are more likely to alternate.

EXPERIMENTAL

The Bis-GMA and TEGDMA monomers (Polysciences), the camphorquinone (CQ) used as photoinitiator, and the *N*,*N*,3,5-tetramethylaniline (TMA) used as promoter (Sigma) were used as received. The CQ (0.2% w/w) was dissolved in the Bis-GMA and the TMA promoter (0.3% w/w) in the TEGDMA. The two parts were mixed at 70/30%w/w proportion to form a homogeneous reacting mixture.

A Q-switched Nd:YAG laser (Continuum) at 532 nm, 10 Hz, 7 ns duration, and pulse energy of about 400 μJ were used for generating the ultrasound waves. The diameter of the irradiated spot was about 1 mm. The PA signals were recorded from the beginning to the end of each photopolymerization reaction. The reacting mixture was poured into a rectangular glass holder ($22 \times 15 \times 2$ mm^3). The front face of the holder with the sample inside was aligned perpendicular to the optical line. To receive the laser pulses an Al foil was placed on the front face of the holder. A piezoelectric sensor (PS, 5 MHz) attached to a digital oscilloscope was fixed on the holder rear face. The PP was induced with 468–480 nm visible light by using a dental lamp (Delux, 75 mW). An optical fiber ($\Phi = 8$ mm) was used to direct the visible light through the glass mold. A

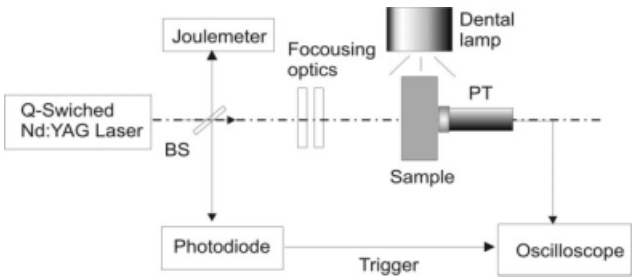

Figure 1 Scheme of the dynamic system used to obtain the PA signals during the photopolymerization of Bis-GMA/TEGDMA (see Refs. 40 and 41). BS, beam splitter, PT, piezoelectric sensor.

scheme of the experimental set up used in this work is shown in Figure 1.

A typical measurement was done as follows: with the visible light source in off position, a recently prepared sample at room conditions is placed in the sample holder; the laser is switched on and the first PA signal is acquired [see 01 signal in Fig. 2(a)], this record is the reference point. Next, the sample is exposed to a 1 s pulse of visible light, through the dental lamp, to initiate the polymerization reaction. Polymerization continues in the dark (after the visible light has been switched off) and the evolution of the polymerization is monitor by the photoacoustic system, acquiring consecutively PA signals [signals 02–12 in Fig. 2(a)]. When no changes are observed between consecutive signals, data acquisition is stopped. Then, another visible light pulse (1 s) is applied on the sample. And again, PA signals are consecutively acquired. This procedure is repeated until the sample is completely polymerized as shown in Figure 2(b). About 55 PA signals were obtained from each sample until completing the photopolymerization process. Each signal, containing 15,000 data points, was normalized and conditioned before the analysis by the fractal methods described in Methods used to study fractal nature section.

The chemical conversion of the Bis-GMA/TEGDMA system was determined under almost the same irradiation conditions set for the PA experiments, by using a (Nicolet spectrometer, model 510P). The detailed procedure is reported elsewhere.[7] The experiment was repeated five times on independent samples to check reproducibility.

RESULTS AND DISCUSSION

As it is well known, network formation by free-radical polymerization of multiunsaturated monomers displays special features of linear polymerization, primarily the occurrence of autoacceleration (gel effect). However, there are several differences arising from the existence of more than one double bond in the monomer molecule.[34] Polymerization of divinyl monomers, in particular, bulk photopolymerization of acrylate-based resins such as Bis-GMA/TEGDMA systems, involves linear chain growing, cyclation by intramolecular crosslinking and network formation by intermolecular crosslinking.

Chemical conversion of the Bis-GMA/TEGDMA system was determined by FTIR, under almost the same irradiation conditions set for the PA experiments, by monitoring the concentration of double bonds as a function of reaction time. Figure 3 shows the photopolymerization average conversion of double bonds as a function of time. Point A sets the beginning of polymerization ($t = 0$). Point B corresponds to the onset of autoacceleration. During Stage A–B, microgel formation occurs as well as branching and intramolecular crosslinking. Autoacceleration causes a rapid increase in the polymerization rate, Stage B–C. In this stage, intermolecular crosslinking leads to network formation. At still higher conversions the gel effect appears to stop and the polymerization rate, R_p, reaches its maximum value. Then the reaction proceeds with decreasing rate, stage C–D, until vitrification is reached, $> E$.

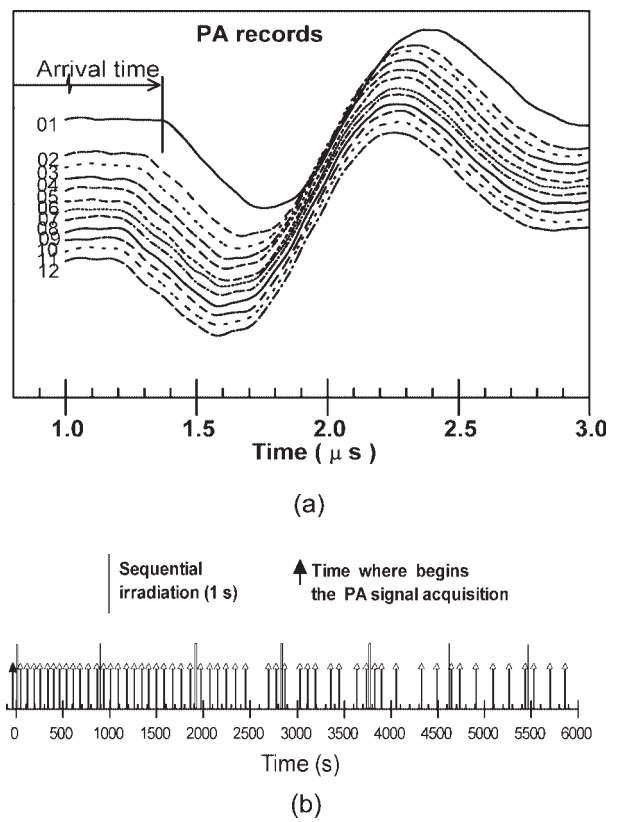

Figure 2 (a) Typical temporal evolution of PA signals obtained from a Bis-GMA/TEGDMA sample. Record 01 is the PA initial response (before irradiating the sample with visible light). Records 02–12 are the signals at different relaxation times after a visible-light irradiation pulse of 1 s. (b) Sequential visible light pulses intervals were between 14 ± 2 min.

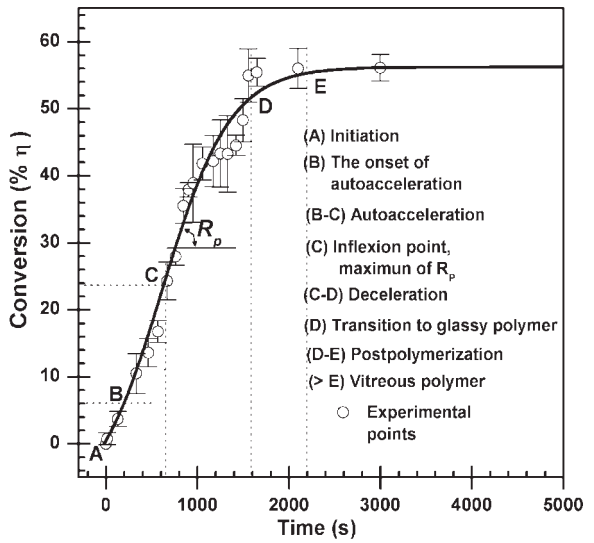

(a)

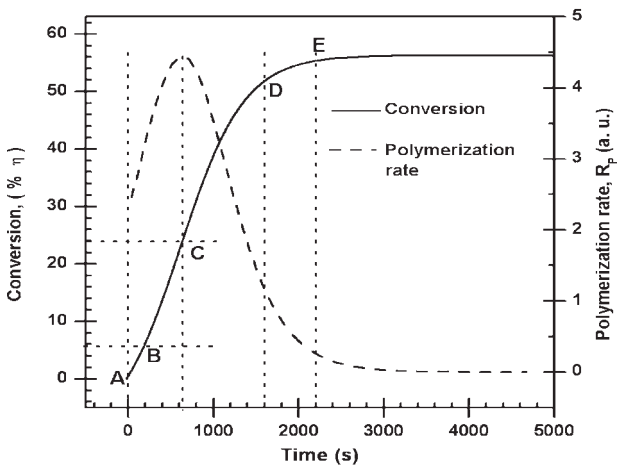

(b)

Figure 3 (a) Conversion (double bonds) as a function of reaction time of a Bis-GMA/TEGDMA sample, in sequential exposures of visible light as shown in Figure 2(a). (b) Fitted conversion curve and polymerization rate (R_P) as a function of reaction time.

The kinetics of the photopolymerization reaction depicted in Figure 3(a,b) will be discussed later, in combination with the results of the fractal analysis.

The initial evolution of the PA signals, registered just after irradiating the sample with a visible light pulse of 1 s, Figure 2(a), did not provide much information except for the arrival time (time of flight) as a function of reaction time. Therefore, a more detailed study of the evolution of the photoacoustic signals was undertaken.

The arrival time of the PA signals as a function of the reaction time of a Bis-GMA/TEGDMA sample after a visible light pulse of 1 s is shown in Figure 4. It is observed as a reduction in the arrival time of the PA signals as the reaction moves forward. This reduction is caused by an increase in the modulus of

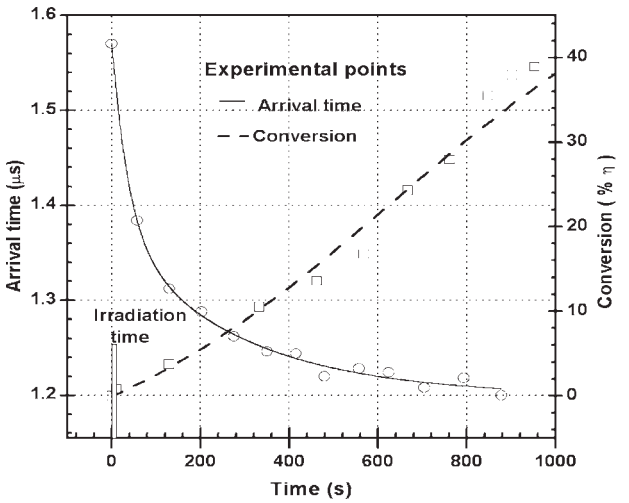

Figure 4 Arrival times of the PA signals as a function of the reaction time of a Bis-GMA/TEGDMA sample after a visible light pulse of 1 s. Conversion of double bonds in the first 1000 s is also shown.

elasticity. After irradiation, the reaction proceeded for about 14 min and reached a conversion near to 40%.

The total arrival time curve, considering all sequential light exposures of the same sample is depicted in Figure 5. In this case, the sample was exposed to seven light pulses, each of 1 s. The time between light exposures was $\sim 14 \pm 2$ min.

The results obtained from each method (R/S, DA, and DFA) used to study fractal development during the curing reaction of Bis-GMA/TEGDMA are discussed later. The plots shown at the left side of Figures 6–8 show Log_{10} (R/S), Log_{10} (SD), and Log_{10}

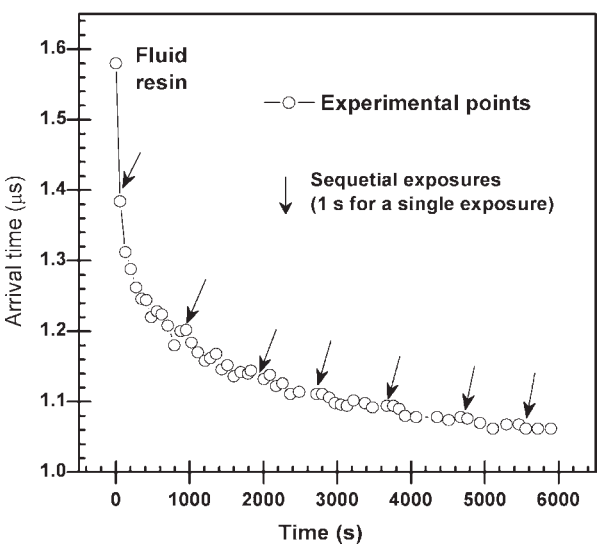

Figure 5 Total arrival time curve for the photopolymerization of a Bis-GMA/TEGDMA sample exposed to a sequential train of irradiation pulses of 1 s each at room conditions.

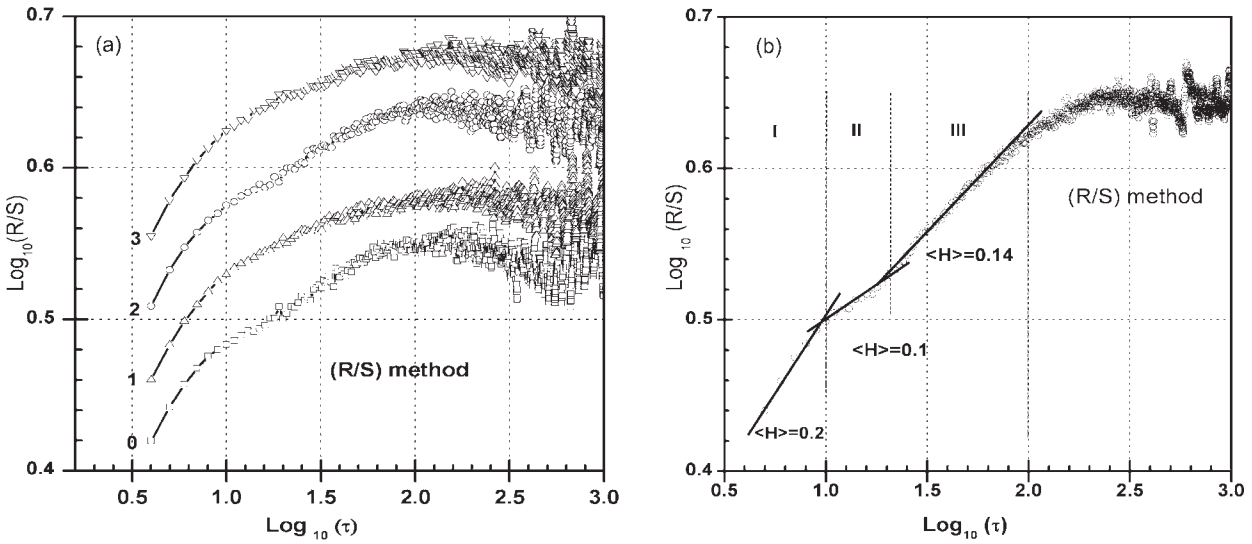

Figure 6 (a) Classic rescaled range, (*R/S*), as a function of box size, τ (b) Fit of $Log_{10}(R/S)$ in linear intervals I, II, and III, in which the scaling parameter <*H*> was divided.

(*F*(*n*)) as a function of box size, respectively. In each plot, the PA signal acquired after the first pulse was used. The plots shown at the right side of Figures 6–8 show the intervals in which the scaling parameter (<*H*> or <α>) was divided. For each set of points a least square linear fit was performed.

Several slope changes were needed to follow the profiles which each model generated. The oscillations observed at the end of the (R/S) and *F*(*n*) profiles are due to the used algorithm. and they are revealed when the box size is too large.[55] As it can be observed, each one of these profiles show at least three different slopes, that define the intervals (I, II, III), indicating the presence of three different time scales for the fractal description of the PA signal. The changes in the slope tell us that there is an <*H*> or <α> value for each interval; meaning the existence of multiple scales. Therefore, these results suggest the presence of multifractality.[55]

Next, the results of the three methods described earlier, now considering all PA signals acquired during the whole PP process, were obtained and compared with the previous results of conversion of double bonds, (η), as a function of photopolymerization time.

The results obtained by the (R/S) method as a function of time are shown in Figure 9 together with conversion of double bonds, (η). Three tendencies, almost linear in <*H*> as a function of time, are observed, in the interval I <*H*> is almost constant,

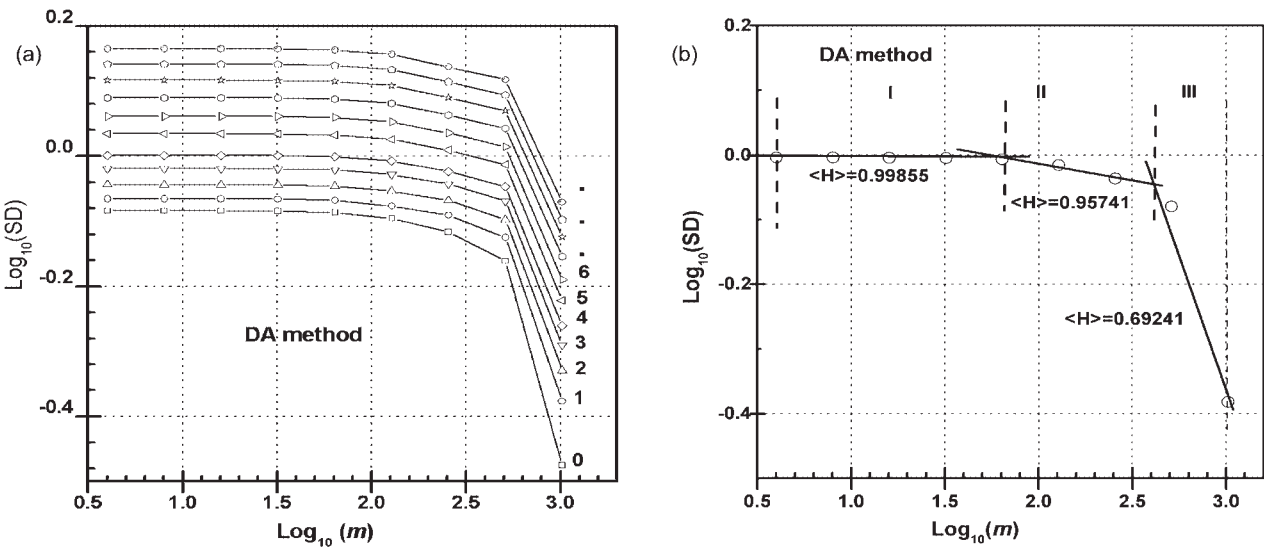

Figure 7 (a) Standard deviation, (SD), as a function of the size element, *m*, (b) Fit of Log_{10} (SD) in linear Intervals I, II, and III, in which the scaling parameter <*H*> was divided.

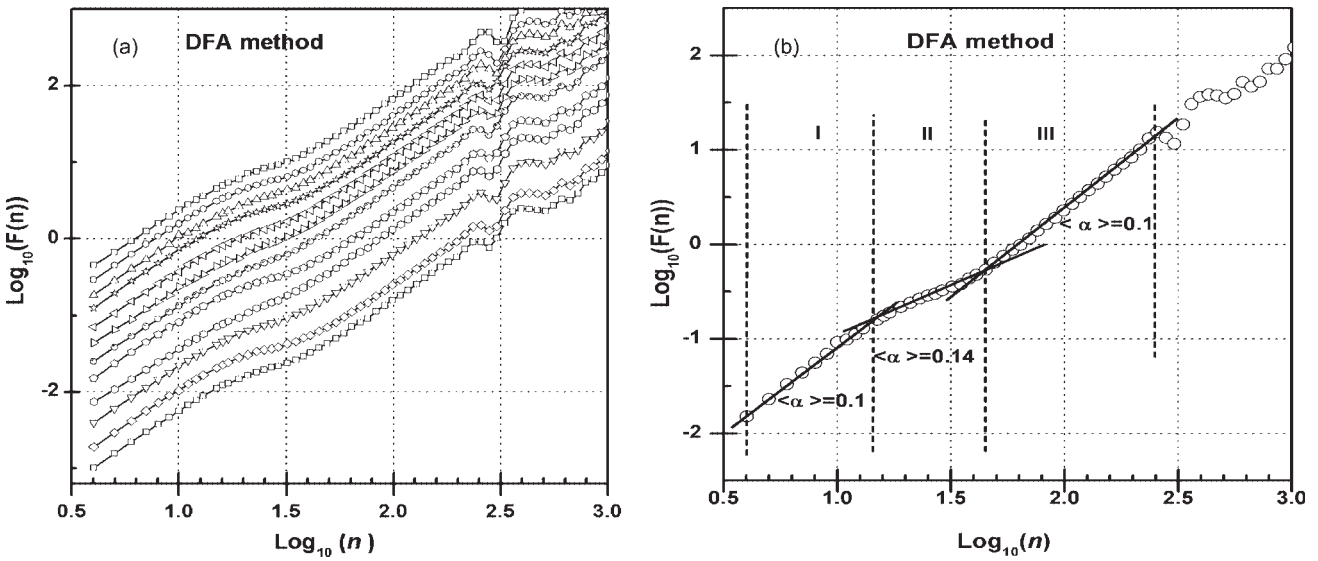

Figure 8 (a) Root mean square fluctuation, Log_{10} ($F(n)$), as a function of box size, (n), (b) Fit of $Log_{10}(F(n))$ in linear intervals I, II, and III, in which the scaling parameter $<\alpha>$ was divided.

although Intervals II and III present high dispersion. As the values $<H>$ are more near to 0 than 0.5 indicate long-term anticorrelated behavior. But, this is because we consider that the PA signals would behave as stationary fractal time series and therefore, as one observes in the Figure 9 the $<H>$ plots do not match with that of (η).

The results obtained by the DA method as a function of reaction time are shown in Figure 10(a). Two lineal tendencies [Intervals I and II in Fig. 7(b)] can be observed, as well as a nonlinear tendency (Interval III) that varies as the reaction advances with a profile more or less similar to that of conversion. The Intervals I and II have a value of $<H>$ near to one, this indicates that the PP process have a long-term correlation. This means that the PA signals have components that behave stationary during the PP process as it was indicated in the previous method. The values of $<H>$ from Interval III shows a dynamical process and of course a component nonstationary in the time series. In this fractal dynamics curve, it is possible to detect phase transitions when they exist. For this reason, the derivative of $<H>$ and conversion, (η), curves were obtained and compared to analyze similarities, they are shown in Figure 10(b). The curve $d\eta/dt$ corresponds to the polymerization rate R_p, whereas the curve $d<H>/dt$ in interval III represents the Hurst Coefficient rate evolution. The R_p curve shows the characteristic features of a free-radical photopolymerization reaction in crosslinking systems (autoacceleration, maximum R_p, and deceleration).[34] The $d<H>/dt$ curve shows a sharp minimum, followed by a maximum, shifted to the right with respect to the point at which R_p reaches its maximum value. The observed minimum in the $d<H>/dt$ curve indicates a structural transition, apparently occurring at the autoacceleration stage.

The results obtained by the DFA method, Figure 11(a), also shows two lineal tendencies [Intervals I and III in Fig. 8(b)] as well as a nonlinear tendency (Interval II) that varies as the reaction advances with a profile similar to that of conversion.

The Intervals I–III have a value of $<\alpha>$ bigger to one, indicating long-term correlations. Under this method, the PA signals almost no have components that behave stationary during the photopolymerization process. The values of $<\alpha>$ from Interval II

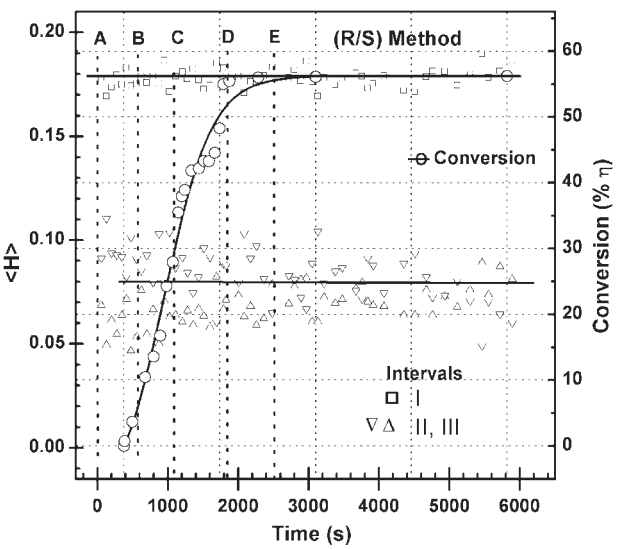

Figure 9 Mean Hurst coefficient, $<H>$, as calculated by the (R/S) method, and chemical conversion, (η), as a function of reaction time.

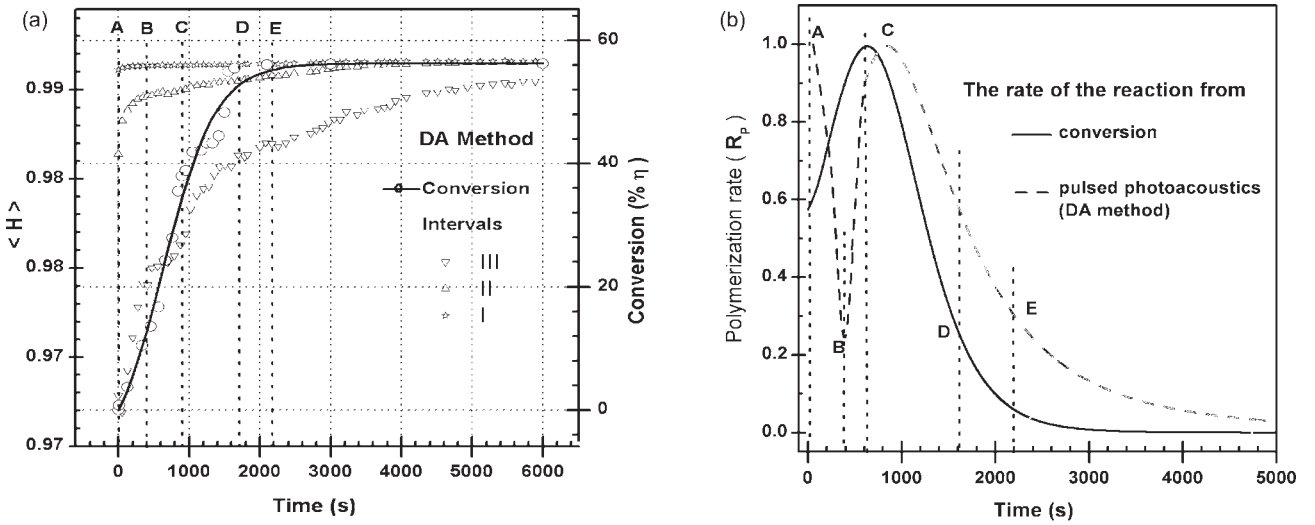

Figure 10 (a) Mean Hurst coefficient, <*H*>, as calculated by the (DA) method, and chemical conversion, (η), as a function of reaction time, (b) derivative of <*H*> and (η) as a function of time.

shows a nonstationary dynamical process in the behavior of the time series. To detect phase transitions or states the derivatives of <α> and conversion curves were obtained as mentioned earlier and compared to analyze similarities, the curve $d<\alpha>/dt$ in interval II represents the self-similarity parameter rate evolution [Fig. 11(b)]. As also mentioned earlier, the R_p plot shows the characteristic features of a free radical photopolymerization reaction in crosslinking systems. The $d<\alpha>/dt$ curve shows two minimums followed by a maximum value of R_p, occurring almost at the same reaction time that R_p reaches its maximum value. The first minimum occurs at the gelation time and second at the end of the autoacceleration stage. These results are clear evidence that both minimums in the $d<\alpha>/dt$ curve represent structural transitions. From models of fractal analysis, Kozlov et al.[31–33] suggested a structural transition occurring at the gel point in crosslinking systems.

According to our results, the DFA method, depicted in Figure 11, properly describes both the evolution of the photopolymerization reaction of Bis-GMA/TEGDMA and its kinetic features. From these results it is clear that the change in fractal nature can be associated with the different stages occurring during in the photopolymerization: microgel formation; network formation with a region of autoacceleration and another region of deceleration; and postcuring. Microgel formation occurs in a liquid state of increasing viscosity, macrogel formation occurs in sol state, and postcuring in vitreous state.

The results also show that during the photopolymerization reaction of Bis-GMA/TEGDMA at least

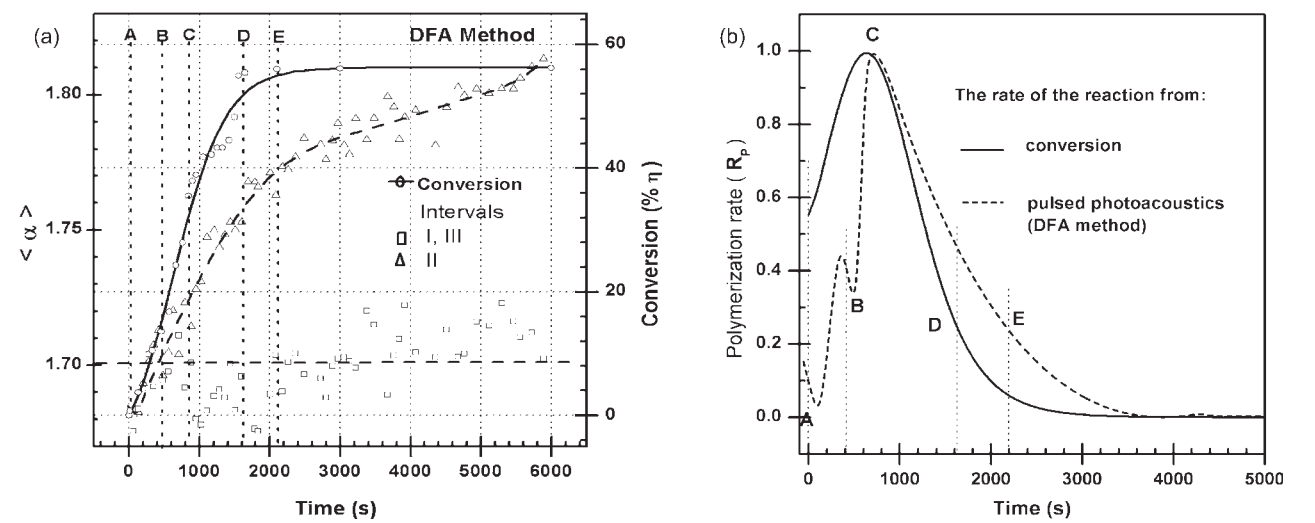

Figure 11 (a) Self-similarity parameter, <α>, as calculated by the (DFA) method, and chemical conversion, (η), as a function of reaction time, (b) derivative of <α> and (η) as a function of time.

two state transitions occur: from homogeneous to heterogeneous at the onset of the autoacceleration, i.e., from viscous to a viscoelastic state (Point B in Fig. 1), and from heterogeneous to homogeneous the onset of vitrification, i.e., from viscoelastic to a vitreous state (Point D in Fig. 1).

CONCLUSIONS

The fractal geometry concept has been introduced to characterize photoacoustic signals acquired during the photopolymerization of a methacrylate comonomer system induced by visible light. The dynamic system used to obtain the photoacoustic signals proved to be successful to monitor *in situ* the change in physical properties during the polymerization reaction of Bis-GMA/TEGDMA.

The multifractal nature during the photopolymerization of Bis-GMA/TEGDMA was resolved by R/S, DA, and DFA.

In our opinion, the DFA method properly describes: The evolution of the photopolymerization reaction; the kinetic stages of the chemical reaction (microgel, autoacceleration and deceleration); and the state transitions occurring during the reaction. In this method, the evolution of the self-similarity parameter also matches with the kinetics of conversion of double bonds.

References

1. Kalachandra, S.; Sankarapandian, M.; Shobha, H. K.; Taylor, D. F.; Mcgrath, J. E. J Mater Sci: Mater Med 1997, 8, 283.
2. Krishnan, V. K.; Manjusha, K.; Yamuna, V. J Mater Sci: Mater Med 1997, 8, 703.
3. Rivera-Torres, F.; Vera-Graziano, R. J Appl Polym Sci 2008, 107, 1169.
4. Lovel, L. G.; Stansbury, J. W.; Syrpes, D. C.; Bowman, C. N. Macromolecules 1999, 32, 3913.
5. Micelli, F.; Maffezoli, A.; Terzi, R.; Luprano, V. A. M. J Mater Sci: Mater Med 2001, 12, 151.
6. Luprano, V. A. M.; Montagna, G.; Molinas, B.; Maffezzoli, A. J Alloys Compd 2000, 310, 382.
7. Vaidyanathan, J.; Vaidyanathan, T. K. J Mater Sci: Mater Med 1992, 3, 19.
8. Decker, C.; Moussa, K. Macromolecules 1989, 22, 4455.
9. Heatley, F.; Pratsitsilp, Y.; McHugh, N.; Watts, D. C.; Devlin, H. Polymer 1995, 36, 1859.
10. Sandner, B.; Kammer, S.; Wartewig, S. Polymer 1996, 37, 4705.
11. Fano, L.; Ma, W. Y.; Marcoli, P. A.; Pizzi, S.; Fano, V. Biomaterials 2002, 23, 1011.
12. Rogers, J. A.; Nelson K. A. Phys B 1996, 219/220, 562.
13. Carothers, W. H. Trans Faraday Soc 1936, 32, 39.
14. Flory, P. J. J Am Chem Soc 1941, 63, 3083.
15. Stockmayer, W. H. J Chem Phys 1944, 11, 45.
16. Flory, P. J. Principles of Polymer Chemistry; Cornell University Press: Ithaca, NY, 1953.
17. Tobita, H. Macromolecules 1993, 26, 5427.
18. Bowman, C. N.; Peppas, N. A. Chem Eng Sci 1992, 47, 1411.
19. O'Shaughnessy, B.; Yu, J. Macromolecules 1994, 27, 5067.
20. O'Shaughnessy, B.; Yu, J. Macromolecules 1994, 27, 5079.
21. Williams, R. J. J; Vallo, C. I. Macromolecules 1988, 21, 2571.
22. Dotson, N. A. Macromolecules 1992, 25, 308.
23. Dušek, K. Br Polym J 1985, 17, 185.
24. Kurdikar, D. L.; Šomvársky, J.; Dušek, K.; Peppas N. A. Macromolecules 1995, 28, 5910.
25. Chiu, Y. Y.; Lee, L. J. J Polym Sci Part A: Polym Chem 1995, 33, 269.
26. Sun X.; Chiu, Y. Y.; Lee, L. J Ind Eng Chem Res 1997, 36, 1343.
27. Botet, R.; Jullien, R.; Kolb, M. Phys Rev A 1984, 30, 2150.
28. Kolb, M. Phys Rev Lett 1984, 53, 1653.
29. Jullien, B.; Botet, R. Aggregation and Fractal Aggregates; World Scientific: Singapore, 1987.
30. Vicsek, T. Fractal Scientific, Growth Phenomena; World Scientific: Singapore, 1989.
31. Kozlov, G. V.; Bejev, A. A. Fractal and Local order in Polymeric Materials; Nova Science Publishers: Huntington, New York, 2001.
32. Kozlov, G. V.; Bejev, A. A.; Lipatov, Y. S. J Appl Polym Sci 2004, 92, 2558.
33. Kozlov, G. V.; Shustov, G. B.; Zaikov, G. E. J Appl Polym Sci 2004, 93, 2343.
34. Andrzejwska, E. Prog Polym Sci 2001, 26, 605.
35. Stansbury, J. W.; Dikens, S. H. Polymer 2001, 42, 6363.
36. Latorre-García, M.; Alvaréz-Gayosso, C.; Barceló-Santana, F.; Vera-Graziano, R. Dent Mater 2006, 22, 1063.
37. Tam, A. C. Rev Mod Phys 1986, 58, 381.
38. Navarrete, M.; Serranía, F.; Villagrán, M.; Bravo, J.; Guinovart, R.; Rodríguez, R. Mech Adv Mater Struct 2002, 9, 157.
39. Mejía-Uriarte, E. V.; Navarrete, M.; Villagrán, M. Rev Sci Instrum 2004, 75, 2887.
40. Navarrete, M.; Rivera, F.; Vera, R.; Villagrán, M. J Phys IV 2005, 125, 749.
41. Rivera, F.; Navarrete, M.; Vera-Graziano, R.; Villagrán, M. J Phys IV 2005, 125, 761.
42. Bassingthwaighte, J. B.; Raymond, M. G. ABME 2006, 94121, 1.
43. Shroeder, M. Fractals, Chaos, Power Laws-Minutes from an Infinite Paradise; W. H. Freeman: NY, 1991; p 429
44. Schmittbuhl, J.; Vilotte, J. P.; Roux, S. Phys Rev E 1995, 51, 131.
45. Hurst, H. E. Trans Am Soc Civ Eng 1951, 116, 770.
46. Barat, P. Chaos Solitons Fractals 1998, 9, 1827.
47. Mandelbrot, B.; Wallis, J. R. Water Resour Res 1969, 5, 228.
48. Mandelbrot, B.; Wallis, J. R. Water Resour Res 1969, 5, 242.
49. Mandelbrot, B.; Wallis, J. R. Water Resour Res 1969, 5, 967.
50. Peng, C. K.; Buldyrev, S. V.; Havlin, S.; Simons, M.; Stanley, H. E.; Goldberger, A. L. Phys Rev E 1994, 49, 1685.
51. Moreira, J. G.; Kamphorst, L. S.; Kamphorst O. J Phys A 1994, 27, 8079.
52. Buldyrev, S. V.; Goldberger, A. L.; Havlin, S.; Peng, C. K.; Stanley, H. E. Biophys J 1993, 65, 2673.
53. Hu, K.; Ivanov, P.; Ch.; Chen, Z; Carpena, P; Santley, E. H. Phys Rev E 2001, 64, 011114.
54. Chen, Z.; Ivanov, P.; Ch.; Hu, K; Stanley, H. E. Phys Rev E 2002, 65, 041107.
55. Cannon, M. J.; Percival, D. B.; Caccia, D. C.; Raymond, G. M.; Bassingthwaighte, J. B. Physica A 1997, 241, 606.
56. Kantelhardt, J. W.; Zschiegner, S. A.; Bunde, A.; Havlin, S.; Koscielny-Bunde, E.; Stanley, H. E. Physica A 2002, 316, 87.
57. Podobnik, B.; Stanley, H. E. Phys Rev Lett 2008, 100, 084102.